Kinks, loops, and protein folding, with protein A as an example

Andrey Krokhotin,[1,a)] Adam Liwo,[2,b)] Gia G. Maisuradze,[3,c)] Antti J. Niemi,[1,4,d)] and Harold A. Scheraga[3,e)]

[1]*Department of Physics and Astronomy and Science for Life Laboratory, Uppsala University, P.O. Box 803, S-75108 Uppsala, Sweden*
[2]*Faculty of Chemistry, University of Gdansk, ul. Sobieskiego 18, 80-952 Gdansk, Poland*
[3]*Baker Laboratory of Chemistry and Chemical Biology, Cornell University, Ithaca, New York 14853-1301, USA*
[4]*Laboratoire de Mathematiques et Physique Theorique CNRS UMR 6083, Fédération Denis Poisson, Université de Tours, Parc de Grandmont, F37200 Tours, France and Department of Physics, Beijing Institute of Technology, Haidian District, Beijing 100081, People's Republic of China*

(Received 23 September 2013; accepted 10 December 2013; published online 8 January 2014)

The dynamics and energetics of formation of loops in the 46-residue N-terminal fragment of the B-domain of staphylococcal protein A has been studied. Numerical simulations have been performed using coarse-grained molecular dynamics with the united-residue (UNRES) force field. The results have been analyzed in terms of a kink (heteroclinic standing wave solution) of a generalized discrete nonlinear Schrödinger (DNLS) equation. In the case of proteins, the DNLS equation arises from a C^{α}-trace-based energy function. Three individual kink profiles were identified in the experimental three-α-helix structure of protein A, in the range of the Glu16-Asn29, Leu20-Asn29, and Gln33-Asn44 residues, respectively; these correspond to two loops in the native structure. UNRES simulations were started from the full right-handed α-helix to obtain a clear picture of kink formation, which would otherwise be blurred by helix formation. All three kinks emerged during coarse-grained simulations. It was found that the formation of each is accompanied by a *local* free energy increase; this is expressed as the change of UNRES energy which has the physical sense of the potential of mean force of a polypeptide chain. The increase is about 7 kcal/mol. This value can thus be considered as the free energy barrier to kink formation in full α-helical segments of polypeptide chains. During the simulations, the kinks emerge, disappear, propagate, and annihilate each other many times. It was found that the formation of a kink is initiated by an abrupt change in the orientation of a pair of consecutive side chains in the loop region. This resembles the formation of a Bloch wall along a spin chain, where the C^{α} backbone corresponds to the chain, and the amino acid side chains are interpreted as the spin variables. This observation suggests that nearest-neighbor side chain–side chain interactions are responsible for initiation of loop formation. It was also found that the individual kinks are reflected as clear peaks in the principal modes of the analyzed trajectory of protein A, the shapes of which resemble the directional derivatives of the kinks along the chain. These observations suggest that the kinks of the DNLS equation determine the functionally important motions of proteins. © *2014 AIP Publishing LLC*. [http://dx.doi.org/10.1063/1.4855735]

I. INTRODUCTION

Proteins come in many shapes. However, the number of different folds seems to be quite limited. For example, the structural classification scheme CATH[1] has thus far identified around 1300 different topologies while in SCOP[2] there are today around 1400 unique folds. These figures have grown very slowly; during the last five years, there have been only nominal changes. Consequently the number of different protein conformations must be relatively limited, and it is possible that the majority have already been found.[3,4]

The great success of CATH, SCOP, and other similar approaches such as FSSP[5] to classify the structure of proteins is a manifestation that proteins are built in a modular fashion and from a relatively small number of different individual modular elements. It has been proposed[6–10] that, mathematically, the modular building blocks of folded proteins can be described by various parameterizations of a kink, or heteroclinic standing wave solution, of a generalized version of the discrete nonlinear Schrödinger (DNLS) equation.[11] The DNLS equation is one of the most fundamental lattice equations. It plays a prominent role in the theories of optical waveguides, photorefractive crystals, Bose-Einstein condensates, particle physics, and string theory.[12–16] The equation describes the stationary points of a Hamiltonian energy function that, in the case of proteins, emerges from general geometric considerations. In fact, it has already been shown that over 92% of high resolution crystals in the Protein Data Bank (PDB)[17] can be

[a)]Electronic mail: Andrei.Krokhotine@cern.ch
[b)]Electronic mail: adam@chem.univ.gda.pl
[c)]Electronic mail: gm56@cornell.edu
[d)]Electronic mail: Antti.Niemi@physics.uu.se
[e)]Electronic mail: has5@cornell.edu

built by combining together no more than 200 different parameterizations of the kink of the DNLS equation as modular elements.[10]

Molecular dynamics (MD) simulations have proven to be a very powerful tool for studying dynamics of protein folding.[18] The accuracy of such simulations depends on the force field used to describe physical interactions within and between peptide units. Force fields range from atomically detailed, in which interatomic interactions are considered explicitly, to coarse grained, in which a simplified description of a polypeptide chain is used and only the most important interactions are usually considered in a simple approximate form. The more detailed the force field is, the more time it takes to run a simulation. Owing to recent hardware and algorithm development such as construction of dedicated machines,[19] use of graphical processing units,[20] or massive use of distributed computing,[21] it is now possible to run all-atom simulations of *ab initio* folding of up to 100-residue proteins at the millisecond scale.[22] Coarse graining enables us to extend this time scale by 3-4 orders of magnitude.[18,23] It must be noted, though, that the present force fields, both atomically detailed and coarse-grained, are far from being accurate. Even small errors in the description of protein energy surfaces can accumulate over a polypeptide chain to disfigure the correct fold.

In this paper, we propose to consider protein folding from another, complementary point of view. Instead of analyzing individual interactions that contribute to the formation of folded structure, we are looking for model-independent principles which are based on symmetry. We suggest that all the physical forces, no matter how strong or weak they are, combine together to give rise to a particular type of protein dynamics, described by a generalized version of the DNLS equation.[6–10] This approach, to much extent, is motivated by methods developed in quantum fields and string theory, in which gauge symmetry was successfully used to derive Hamiltonians of many fundamental forces.[16] We use the united residue (UNRES) force field developed in our laboratory[24–32] to run simulations, to test and confirm our general considerations.

We selected the N-terminal part of the B-domain of staphylococcal protein A as the test case (PDB code: 1BDD). The fold of this protein is a three-α-helix bundle.[33] The folding and energy landscape of this protein were subject to a variety of experimental[34–36] and theoretical[37–45] studies. The version of UNRES used in our study folds α-helical proteins in unrestricted folding simulations,[27] including protein A. Our extensive studies of the free-energy landscape of this protein[44] simulated with the force field used in this study have repeatedly shown that the native three-α-helix bundle is its free-energy minimum and forms a large basin in the free-energy landscape. Another reason to use protein A as the test case was that it was not used in force-field parameterization[27] and the force field is, therefore, not biased to reproduce its native structures (as opposed to the Gō-like models, which are constructed to locate the native structure of the protein under study as the global energy minimum).

The article is organized as follows. In Sec. II A, the geometry of coarse-grained polypeptide chains is defined and new visualization techniques, which are exploited further in the article, are introduced. In Sec. II B, it is argued that protein secondary structures can be described by a kink of the generalized DNLS equation, similar in shape to the hyperbolic-tangent function. This solution of the DNLS equation is the basic modular element that is used here to describe the geometry of a folded protein. An entire protein loop structure is obtained by joining together several kinks in a modular fashion, one after the other, and in combination with those stationary points of the DNLS Hamiltonian that have a well defined secondary structure (such as α-helices and β-strands). In Sec. III A, the previously developed technique is used to describe protein A. In Secs. III B 1 and III B 2, the kink is studied based on the results of coarse-grained simulations with the UNRES force field. In Sec. III C, the behavior of side chains is interpreted as that of spins in spin-chain models. In Sec. III D, mechanisms that cause loop formation are proposed. Finally, in Sec. III E, the profiles of the kinks are compared to those of the principal modes in principal-component analysis (PCA).

II. METHODS

A. Protein backbone geometry and local conformational states

In this paper, protein-backbone geometry is described in terms of Frenet frames.[46] The frames depend *only* on the positions of the C^α carbon coordinates $\mathbf{r}_i$ where $i = 1, \ldots, n$ labels the residues. At a given residue, the frame is defined by the unit backbone tangent ($\mathbf{t}$), binormal ($\mathbf{b}$), and normal ($\mathbf{n}$) vectors, which are defined by Eqs. (1), (2), and (3), respectively; see Figure 1 for graphical illustration:

$$\mathbf{t}_i = \frac{\mathbf{r}_{i+1} - \mathbf{r}_i}{|\mathbf{r}_{i+1} - \mathbf{r}_i|}, \tag{1}$$

$$\mathbf{b}_i = \frac{\mathbf{t}_{i-1} \times \mathbf{t}_i}{|\mathbf{t}_{i-1} \times \mathbf{t}_i|}, \tag{2}$$

$$\mathbf{n}_i = \mathbf{b}_i \times \mathbf{t}_i, \tag{3}$$

where $\mathbf{r_i}$ is the position of the C^α atom of ith residue.

Because the distance between the consecutive C^α atoms is nearly constant so that $|\mathbf{r}_{i+1} - \mathbf{r}_i| \approx 3.8$ Å for *trans* peptide groups, the backbone geometry can be described in terms of virtual-bond-valence angles θ and virtual-bond-dihedral (torsion) angles γ. These angles are the discrete versions of the

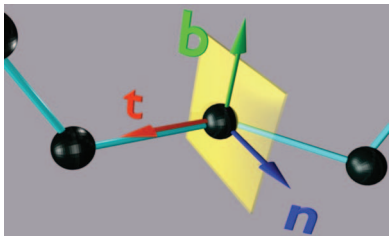

FIG. 1. Definition of Frenet frame. Vector **t** (the transversal or tangent vector) points from a given polymer-chain bead to the next bead. Vector **n** (the normal vector) is perpendicular to **t** and lies in the plane of the preceding, current, and next polymer-chain bead, pointing towards the preceding bead. Vector **b** (the binormal vector) forms the right-handed coordinate system with the transversal vector and the normal vector.

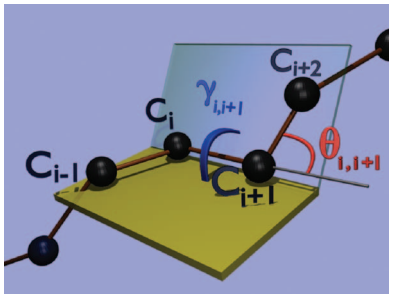

FIG. 2. Definitions of the backbone virtual-bond angle ($\theta_{i,\,i+1}$) and virtual-bond-torsion angle ($\gamma_{i,\,i+1}$) in terms of the C^{α} atoms.

intrinsically geometric curvature and torsion of a continuous space curve. The complements of the angles θ and the angles γ are defined by Eqs. (4) and (5), respectively:

$$\theta_{i+1,i} \equiv \theta_i = \arccos(\mathbf{t}_{i+1} \cdot \mathbf{t}_i), \tag{4}$$

$$\gamma_{i+1,i} \equiv \gamma_i = \omega \arccos(\mathbf{b}_{i+1} \cdot \mathbf{b}_i), \tag{5}$$

with

$$\omega = \mathrm{sgn}[(\mathbf{b}_{i-1} \times \mathbf{b}_i) \cdot \mathbf{t}_i]. \tag{6}$$

These angles are also illustrated in Figure 2.

The frame vectors can be expressed in terms of the virtual-bond-valence angles θ and virtual-bond-dihedral angles γ by Eq. (7) and then the C^{α}-trace geometry can be calculated from Eq. (8):

$$\begin{pmatrix} \mathbf{n_{i+1}} \\ \mathbf{b}_{i+1} \\ \mathbf{t}_{i+1} \end{pmatrix} = \begin{pmatrix} \cos\theta\cos\gamma & \cos\theta\sin\gamma & -\sin\theta \\ -\sin\gamma & \cos\gamma & 0 \\ \sin\theta\cos\gamma & \sin\theta\sin\gamma & \cos\theta \end{pmatrix}_{i+1,i} \begin{pmatrix} \mathbf{n_i} \\ \mathbf{b}_i \\ \mathbf{t}_i \end{pmatrix}, \tag{7}$$

$$\mathbf{r}_k = \sum_{i=0}^{k-1} |\mathbf{r}_{i+1} - \mathbf{r}_i| \cdot \mathbf{t}_i. \tag{8}$$

We may assume that the distance between two consecutive C^{α} atoms is constant, and given by

$$|\mathbf{r}_{i+1} - \mathbf{r}_i| = \Delta \approx 3.8\,\text{Å}.$$

This is a good approximation, as long as there are no *cis*-residues.

It should be noted that, unlike the tangent vector $\mathbf{t}_i$, the normal and binormal vectors ($\mathbf{n}_i$, $\mathbf{b}_i$) do not appear in Eq. (8). Therefore, if these vectors are simultaneously rotated around the vector $\mathbf{t}$, they constitute a good reference system. In particular, rotation by π constitutes the discrete $\mathbb{Z}_2$ gauge transformation [Eq. (9)], which was used extensively in our earlier work[6–10,46] and will also be utilized in this work:

$$\begin{aligned} &\theta_i \rightarrow \theta_i - \pi, \\ &\gamma_k \rightarrow -\gamma_k \quad \text{for all } k \geq i. \end{aligned} \tag{9}$$

If the (θ, γ) angle pairs are identified with polar coordinates, local conformational states of amino-acid residues can be mapped onto a sphere and then stereographically projected

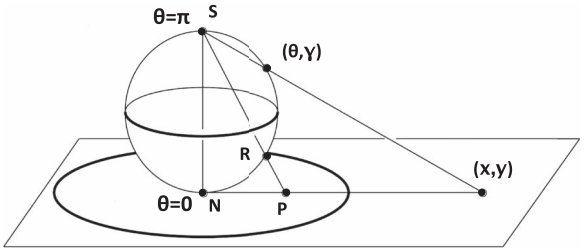

FIG. 3. Two-sphere with its stereographic projection onto the plane. The point (θ, γ) on the surface of the sphere is mapped onto the point (x, y) on the plane, as expressed by Eq. (10). N and S are the north and south poles, respectively.

onto a disk, as shown in Figure 3. The stereographic projection is obtained by projecting the (θ, γ) coordinates onto the north-pole tangent plane of the two-sphere. If (x, y) are the coordinates of this tangent plane, the projection is defined by Eq. (10):

$$x + iy = \tan\left(\frac{\theta}{2}\right) \cdot e^{-i\gamma}. \tag{10}$$

The statistical distribution for all PDB proteins in the stereographically projected two-sphere, for those conformations that have been determined at resolution higher than 2.0 Å is shown in Figure 4. Two regions corresponding to the right-handed α and to the β structure can be distinguished. In Figure 4(b), a generic loop is depicted that connects two right-handed α-helical structures. A generic loop is a pathway that

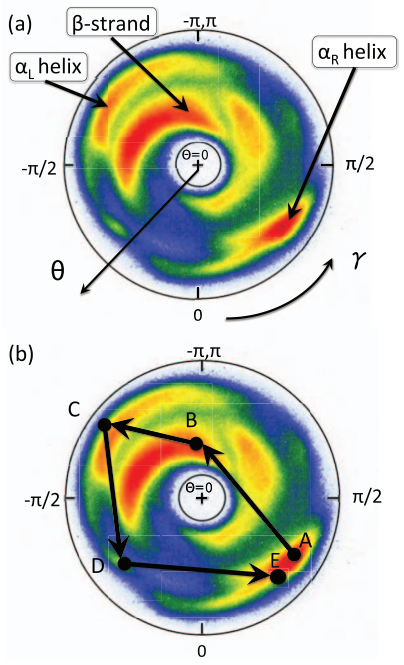

FIG. 4. (a) The distribution of bond and torsion angles on the stereographically projected two-sphere (θ, γ); see Figure 3 for definition of the projection. The color intensity is (logarithmically) proportional to the number of PDB entries (red > yellow > green > blue > white). (b) An example of a circular path (corresponding to a loop structure), as an oriented trajectory on the stereographically projected two-sphere. The circular path starts from the right-handed α-helical region (A), proceeds to the β-strand region (B), to the left-handed α region (C), followed by steps (D) and (E), and terminates in region of the right-handed α-helical region (A).

connects the adjacent regular secondary structures; the latter corresponds to point-like structures in the map, *i.e.*, constant values of (θ_i, γ_i). For example, parameter values (in radians) for which

$$\begin{cases} \theta_i \approx \frac{\pi}{2} \\ \gamma_i \approx 1 \end{cases} \tag{11}$$

describe a right-handed α-helix, and parameter values for which

$$\begin{cases} \theta_i \approx 1 \\ \gamma_i \approx \pm\pi \end{cases} \tag{12}$$

describe a β-strand.

A notable property of the trajectory drawn in Figure 4(b) is that it encircles the north-pole of the two-sphere. It turns out that this kind of encircling is quite generic for loops. Consequently, each loop can be assigned a winding number termed *folding index*, Ind_f,[47] which is defined by Eq. (14):

$$Ind_f = \left[\frac{\Gamma}{\pi}\right], \tag{13}$$

$$\Gamma = \frac{1}{\pi}\sum_{i=n_1+2}^{n_2-2} \begin{cases} \gamma_{i,i+1} - \gamma_{i-1,i} - 2\pi & \text{if } \gamma_{i,i+1} - \gamma_{i-1,i} > \pi \\ \gamma_{i,i+1} - \gamma_{i-1,i} + 2\pi & \text{if } \gamma_{i,i+1} - \gamma_{i-1,i} < -\pi \\ \gamma_{i,i+1} - \gamma_{i-1,i} & \text{otherwise} \end{cases}, \tag{14}$$

where $[x]$ denotes the integer part of x, and Γ is the total rotation angle (in radians) that the projections of the C^α atoms of the consecutive loop residues make around the north pole. The folding index is a positive integer when the rotation is counterclockwise and a negative integer when the rotation is clockwise. The folding index classifies loop structures and entire folded proteins in terms of its values. The value is equal to twice the number of times the ensuing pathway encircles the north-pole in the map of Figure 4.

Using the Frenet frame, the C^β atoms can also be visualized in the unit two-sphere system centered at the C^α atom with the axis **t** chosen as the polar (z) axis and the axes **n** and **b** chosen as the x and y axes, respectively, to define a right-handed coordinate system. The canonical spherical coordinates (ϑ_i, φ_i) are introduced, which are essentially the bond angle θ and torsion angle γ, respectively. Like the angle θ, the angle $\vartheta \in [0, \pi]$ measures the latitude from the positive z-axis and the angle $\varphi \in [0, 2\pi]$ now measures the longitude in a counterclockwise direction from the x-axis, *i.e.*, from the direction of **n** towards that of **b**. Then the coordinates of a unit vector $\mathbf{s}_i$ pointing from C^α in the direction of C^β can be computed from Eq. (15):

$$\mathbf{s}_i = \begin{pmatrix} \cos\varphi_i \ \sin\vartheta_i \\ \sin\varphi_i \ \sin\vartheta_i \\ \cos\vartheta_i \end{pmatrix}. \tag{15}$$

As shown in Figure 5, the direction of the vector $\mathbf{s}_i$, computed from PDB structures, is quite well defined, with one major and one minor cluster subdivided into regions corresponding to α_R and β structures and one minor region corresponding to the left-handed α-helical (α_L) structures. For the

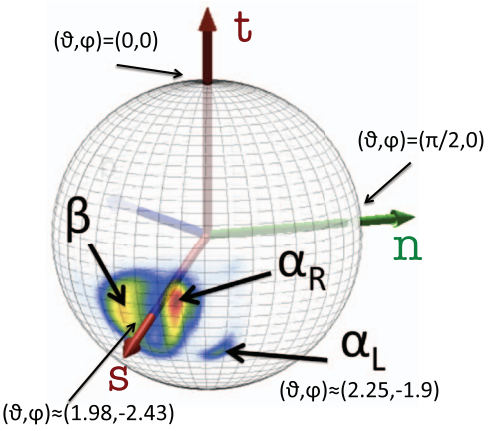

FIG. 5. Statistical distribution of the C^β direction in the PDB, as seen from the corresponding C^α, located at the center of the sphere. The vector **t** points towards the next C^α. The regions of right-handed α_R-helices, β-sheets, and left-handed α_L are displayed, the rest being non-regular structures (including loops). The (average) vector **s** is also shown.

major cluster, the average latitude angle ϑ_i is $\langle\vartheta\rangle \approx 1.98$ rad and the average value of the longitude angle φ is $\langle\varphi\rangle \approx -2.43$ rad; these values undergo only small fluctuations. The average values of the spherical angles for the α_L region are $\langle\vartheta\rangle \approx 2.25$ rad and $\langle\varphi\rangle \approx -1.90$ rad, respectively. Thus, the orientation of the C^β atom is quite well defined in a given frame of three consecutive C^α atoms and, consequently, the positions of C^β atoms can be determined quite accurately given the C^α trace.

B. Kink of the DNLS equation and protein geometry

As noted in Sec. II A, the C^α trace geometry can be described in terms of the virtual bond and virtual torsion angles [Eqs. (4) and (5)]. For a coarse-grained description of the side-chain orientations, the vector from the C^α to the ensuing side-chain centroids can be utilized. These variables are present in the UNRES energy function.[24–32] Alternatively, the vector from the C^α atom to its side-chain C^β atom [vector **s** of Eq. (15)] can be used. As follows from Figure 5, the direction of vector **s** is essentially constant and independent of amino-acid type. Consequently, the backbone geometry largely determines the side-chain orientations and, thus, the complete geometry of polypeptide chains at the coarse-grained level.

In the case of a protein, the variables θ_i and γ_i are mutually connected by the equations of motion, determined by the atomic level interactions along the protein chain. In Refs. 6, 7, 9 and 10 (see also Ref. 48 in the present context), the following Landau energy has been introduced to approximate the Helmholtz free energy F of the protein backbone in terms of the discrete virtual bond and torsion angles:

$$F = -\sum_{i=1}^{N-1} 2\,\theta_{i+1}\theta_i + \sum_{i=1}^{N}\Big\{2\theta_i^2 + \lambda\,(\theta_i^2 - m^2)^2 + \frac{q}{2}\,\theta_i^2\gamma_i^2 - p\,\gamma_i + \frac{r}{2}\gamma_i^2\Big\}. \tag{16}$$

In addition, the excluded volume (steric) constraint

$$|\mathbf{r}_i - \mathbf{r}_k| \geq 3.8\ \text{Å} \quad \text{for} \quad |i-k| \geq 2 \tag{17}$$

is imposed, for the distance between the backbone C^α atoms. This condition is well respected by folded protein structures in the PDB. In Eq. (16), λ, q, p, r, and m are parameters. The free energy, Eq. (16), has been derived and motivated in detail in Refs. 6, 7, 9 and 10. Here it suffices to state that this free energy can be shown to relate to the long-distance limit that describes the full microscopic energy of a folded protein in the universal sense of Refs. 49–52. As such, it does not explain the details of the (sub)atomic level mechanisms that give rise to protein folding.

A C^α backbone conformation is constructed by seeking the minimum of F in Eq. (16).[6,7,9,10] The necessary condition for the minimum is to find the zero of the gradient of F in the virtual-bond angles θ and in the virtual-bond dihedral angles γ. The solution of this problem is the solution of a system of $2N-5$ nonlinear equations in $2N-5$ unknowns (where N is the number of residues). In order to obtain this solution, the virtual-bond-dihedral angles γ are first expressed as functions of the virtual-bond angles θ, as given by Eq. (18):

$$\gamma_i[\theta] = \frac{p}{r + q\,\theta_i^2} \equiv \frac{u}{1 + v\,\theta_i^2}, \tag{18}$$

with $u = p/r$ and $v = q/r$. By inserting Eq. (18) into Eq. (16), the virtual-bond-dihedral angles γ are eliminated and a system of equations (19) for the motion of the virtual-bond angles θ is obtained:

$$\theta_{i+1} = 2\theta_i - \theta_{i-1} + \frac{dV[\theta]}{d\theta_i^2}\theta_i \quad (i = 1, \ldots, N), \tag{19}$$

where $\theta_0 = \theta_{N+1} = 0$ and

$$V[\theta] = \frac{p}{r + q\,\theta^2} + 2(1 - \lambda m^2)\theta^2 + \lambda\,\theta^4, \tag{20}$$

where the structure of the generalized DNLS equation with a double-well potential that describes discrete symmetry, that has been spontaneously broken,[15,16] is recognized.[6–10] The kink solution to Eq. (19) can be constructed numerically by following the iterative procedure of Ref. 7. But its explicit form, until now, has not been found in terms of elementary functions. However, an *excellent* approximation is obtained by *naively* discretizing the heteroclinic standing wave solution to the continuum nonlinear Schrödinger equation[6–10]

$$\theta_i = \frac{b\,\exp[\sigma_1(i-s)] + a\,\exp[-\sigma_2(i-s)]}{\exp[\sigma_1(i-s)] + \exp[-\sigma_2(i-s)]}. \tag{21}$$

Here s is a parameter that determines the center of the solution. The $a, b \in [0, \pi] \bmod(2\pi)$ are parameters which determine the amplitude of the variation of θ and the asymmetry of the inflection regions; they correspond to the two minima of the potential energy contribution $V[\theta]$ in Eq. (20). The θ angle profile given by Eq. (21) is like a localized domain wall, which describes the boundary between two neighboring minima of the potential energy.[15,16] The parameters σ_1 and σ_2 are related to the inverse of the range of the kink. It is notable that, in the case of proteins, the values of a, b are determined entirely by the adjacent helices and strands. Far away from the center of the kink we have (see Figure 6)

$$\theta_i \to \begin{cases} b \mod(2\pi) & i > s \\ a \mod(2\pi) & i < s \end{cases}$$

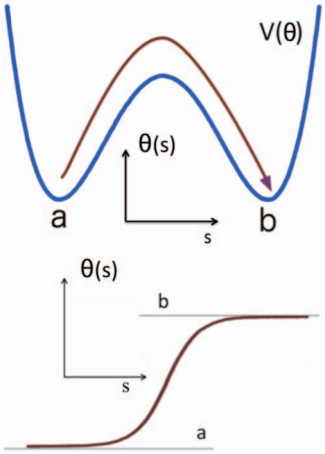

FIG. 6. Top: The potential of mean force (PMF) of θ. Bottom: The kink [Eq. (21)] is the boundary between two neighboring local minima $s = a$ and $s = b$ of the PMF.

and, according to Eqs. (11) and (12), the asymptotic values

$$\theta_i \approx \pi/2 \text{ or } -\pi/2 \quad \text{and} \quad \theta_i \approx 1 \text{ or } 1 - \pi$$

correspond to the α-helix or β-strand, respectively. A kink corresponding to a loop connecting two α-helices in the helix-turn-helix motif is illustrated in Figure 7. It should be noted that, in the case of proteins, negative values of θ_i are related to positive values of θ_i by Eq. (9). Moreover, in the case of proteins, to satisfy the monotonic character of the profile of Eq. (21), the experimentally measured values of θ_i have to vary monotonically along the amino-acid sequence. Otherwise, a multiple of 2π is added to the experimental values. This does not affect the backbone geometry because θ_i's are defined $\bmod(2\pi)$.

Finally, *only* σ_1 and σ_2 are intrinsically specific parameters for a given loop in Eq. (21). But they specify only the length of the loop, not its shape which is determined by the functional form of Eq. (21) and, as in the case of a and b of Eq. (21), they are combinations of the parameters in Eq. (20).

The corresponding virtual-torsion angles $\gamma_i, i = 1, 2, \ldots, N-3$, are evaluated in terms of the bond angles using Eq. (18). In Eq. (18) for the virtual-torsion angles, there are

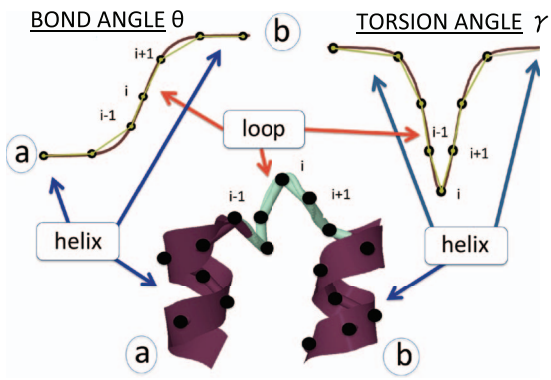

FIG. 7. Top: Schematic sketches of the profiles of angles θ (left) and γ (right) along the chain. Bottom: The solutions of the generalized DNLS equation are the modular building blocks of folded proteins. They correspond to super-secondary structures such as right-handed-α-helix-loop-right-handed-α-helix (strand-loop-strand).

only two independent parameters u and v. As a consequence, the profile of γ_i is determined entirely by the profile of θ_i, and on the structure of the adjacent regular secondary structures.

It has been shown[9] that most protein loop structures from the PDB (over 92% of them) can be described in terms of the explicit profile Eq. (21) in combination with Eq. (18) along with the parameters of these equations, as the elemental modular components, with a root-mean-square-deviation (RMSD) precision which is better than 0.6 Å. This is strong support for the proposal[6,7,9,10] that the kink correctly describes the protein structures in the PDB.

At present, we do not consider the kinks in terms of protein-structure prediction but as a convenient tool to describe protein structure. As mentioned in the Introduction, we have already proved that loop geometries of the protein structures present in the PDB can be described in terms of 200 sets of the parameters of the DNLSE.[10] Nevertheless, in our earlier work[10] we have also demonstrated that, using the kink parameters extracted from the experimental structure of a protein, its folding can be simulated.

Kink analysis seems to handle the description of the conformations that do not occur in the PDB. In our earlier work,[48] we studied the AICD/Fe65 complex by means of kink analysis (in that paper referred to as soliton analysis) and coarse-grained simulations with UNRES. The kinks in the AICD part of the complex, when propagated according to the solution of the DNLSE, resulted either in the formation of the compact structure (favorable for the single components) or even more unfavorable partially extended structure that could be amyloid precursor.

C. Coarse-grained dynamics simulations

To study formation of the structures described by the kink solution of Eq. (19) in proteins, canonical coarse-grained dynamics simulations of the 10-55 fragment of protein A were carried out with the UNRES package developed in our laboratory[24–28,30–32] available at http://www.unres.pl. The MD protocol described in our earlier work[18,23,53] was used. Sixteen parallel trajectories, started from complete right-handed α-helical structures, were run at each of the following temperatures: T = 150, 200, 240, 250, 300, and 310 K. 20 000 000 steps were run for each trajectory with the time step $\delta t = 4.89$ fs. This trajectory length corresponds to 98.8 ns UNRES time, but because the time scale in UNRES/MD is distorted at least 1000 times compared to all-atom MD with explicit water,[23,53] the effective duration of simulations was about 0.1 ms. Constant temperature was maintained with the use of the Berendsen thermostat[54] with the coupling parameter $\tau = 48.9$ fs. The version of the UNRES force field parameterized with the 1GAB training protein was used;[27] this force field is good for simulating the structure and dynamics of α-helical proteins.[27]

III. RESULTS AND DISCUSSION

A. An analysis of the experimental structure of protein A in terms of kinks

We carried out a detailed analysis of protein-loop formation, using the N-terminal segment of the B-domain of staphylococcal protein A as an example. Our analysis relies on quite general, universal concepts and, consequently, it can be argued that the results are generic. The 1BDD experimental structure[33] was taken as the reference. This is an average nuclear magnetic resonance (NMR) structure. Of the 60 residues present in the experimental structure, a 46-residue fragment (residues Gln10-Asn55 of the PDB structure) was selected, after removing the unstructured N-terminal and C-terminal residues. In Figure 8, both the full 1BDD backbone and the 46-residue Gln10–Ala55 are shown.

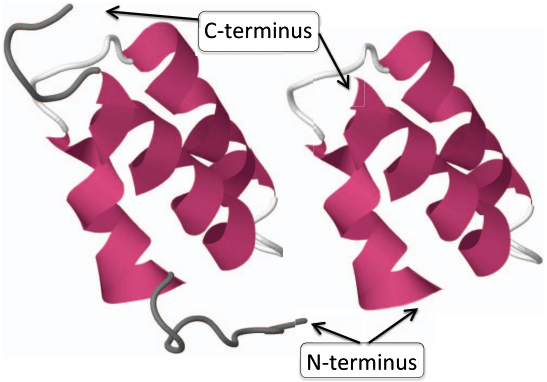

FIG. 8. On the left, the full PDB structure 1BDD, and on the right the 46-residue segment substructure Gln10-Ala55 studied in detail. The dark grey areas in the figure on the left are the unstructured N and C tails that have been removed.

1. Kink structure of 1BDD

We start by resolving the kink structure of 1BDD, using the explicit profile given by Eq. (21). Variations of the angles θ and γ along the chain are shown in Figure 9(a), with the convention that the bond angle is always positive. For the most part, the bond and torsion angles fluctuate in the

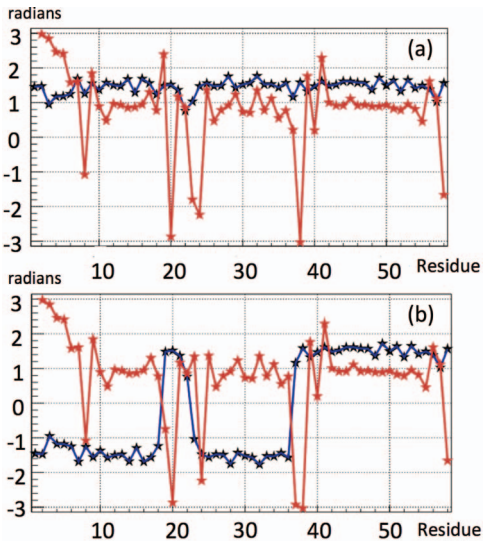

FIG. 9. The virtual-bond θ_i (black) and torsion γ_i (red) angle spectra of 1BDD. Figure 9(a) uses the convention that the bond angle is positive. In Figure 9(b), we have introduced the $\mathbb{Z}_2$ transformation [Eq. (9)] to reveal the kink content at the peaks.

vicinity of the standard right-handed α-helical values ($\theta \approx \pi/2$, $\gamma \approx 1$). However, there are two regions, located between Ile17–Asn24 and Gln33–Ala43, respectively, where in particular the virtual-bond-dihedral angle γ_i is subject to large fluctuations.

In Figure 9(b) the discrete $\mathbb{Z}_2$ transformation [Eq. (9)] was applied to the data in Figure 9(a), to resolve the kink content of the backbone: There is a putative conformation, described by a combination of two kinks of Eq. (21) in succession, located in the segment between PDB C^α sites Ile17 and Asn24. The putative first kink is centered between PDB C^α sites Leu20 and Pro21, and the putative second kink is centered at Asn24–Glu25. Together, these two kinks constitute the first loop structure of 1BDD. The second loop structure consists of a single kink, which is centered between residues Asp38 and Pro39.

The fact that a loop is described by two kinks tells us that it consists of two half-turns, which form roughly an "open rectangle with rounded edges" shape, as opposed to an approximate "U" shape created by one kink (see the blue plot in Figure 9(b), in the region of Ile17–Asn24 and Gln33–Ala43, respectively, and the structures corresponding to these regions in Figure 10).

2. Kink profiles

We have confirmed [Figure 9(b)] that the interpretation of 1BDD in terms of one kink pair and an isolated kink solution of DNLS equation is correct, by fitting the profile to the discretized form of Eqs. (21) and (18). The parameter values are listed in Table I. Equations (21) and (18) describe the first kink with RMSD precision of 0.12 Å, the second kink with RMSD precision 0.31 Å, and the third kink with RMSD precision 0.47 Å. In Figure 10 the ensuing conformations, interlaced with the PDB structure of protein A (1BDD) are displayed. It can be concluded that the interpretation of protein A as a combination of three kinks is fully consistent with Eqs. (18)–(21) that we have derived from the Helmholtz free energy of Eq. (16).

3. Folding index

The (θ_i, γ_i) trajectories of the three kinks of 1BDD in the stereographically projected hemisphere are shown in

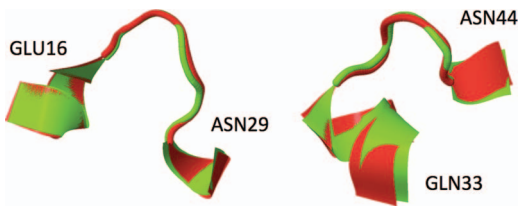

FIG. 10. The kink representation for the two loops of protein A (red) interlaced with the 1BDD structure (green). On the left, the first two kinks, on the right the third kink. The first kink covers sites Glu16-Asn22, the RMSD from the experimental 1BDD structure being 0.12 Å. The second kink covers sites Leu20-Asn29, the RMSD with respect to the experimental 1BDD structure being 0.31 Å. The third kink covers sites Gln33-Asn44, the RMSD from 1BDD being 0.47 Å.

TABLE I. Best parameter values for each of the three kinks in protein A.[a] Note that the angular variables are dimensionless; thus, these parameters are also dimensionless.

Parameter	Kink-1	Kink-2	Kink-3
a	− 33.0096	− 20.3583	− 45.5178
b	33.0784	20.346	45.4973
σ_1	2.2082	2.5755	2.9127
σ_2	2.2064	2.5837	2.9221
s	18.4962	22.1432	37.9139
u	976012.94	− 311747.469	− 5669135.02
v	− 0.00098719	− 0.00158963	− 0.00021636

[a]It should be noted that a, b are determined mod (2π).

Figures 11(a)–11(c). The putative first kink (Figure 11(a)) located at Leu20–Pro21 rotates counterclockwise. But, since it does not extend around the center, there is no contribution to the folding index. The second putative kink at Asn24–Glu25 (Figure 11(b)) rotates clockwise around the center once, and consequently it contributes −2 to the normalized folding index defined by Eq. (14)[47] (i.e., the loop makes one turn

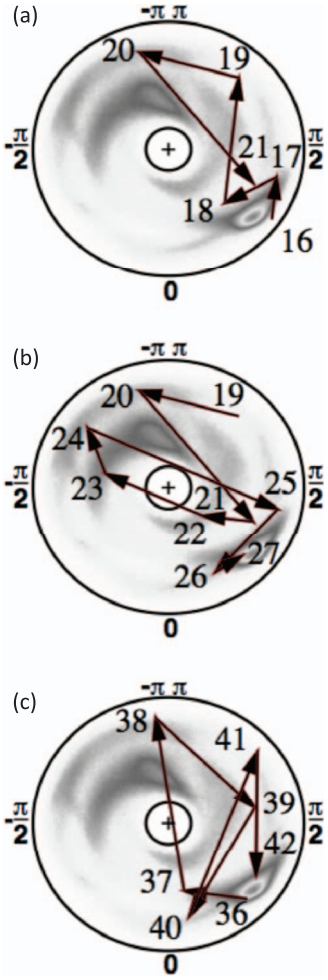

FIG. 11. The folding index trajectories for the three loop structures of 1BDD identified in Figure 8. The quality of the data of 1BDD is not optimal. But it appears that in (a), a trajectory tries to go around the center once, in a counterclockwise fashion. In (b) and (c), the circulation is once in a clockwise direction. As a consequence, the kink contribution to the folding index of fully folded protein A should be −2.

around the north pole). Finally, for the Asp38-Pro39 region (Figure 11(c)) the folding index is unstable. A tiny fluctuation of the coordinates of Asp37 or Asp38 to avoid crossing the center causes the normalized folding index either to vanish, or acquire, the value +2. As a consequence, on average, the value of the folding index vanishes.

Except for the second kink, the quality of the experimental structure is not good enough to eliminate the effect of fluctuations in the folding index. But an inspection of Figure 11 proposes that the first kink located at Leu20–Pro21 should have (integer part of) folding index equal to +2 as the vector field rotates once around in a counterclockwise direction. Similarly the third kink should make a contribution of −2 to the folding index, as the vector field makes one full clockwise turn. Consequently, the three kinks should contribute a total of

first kink	second kink	third kink	whole chain
+2	−2	−2	= −2

to the total folding index.

We note that, for the entire chain, including the flexible portions near the N and C tails, we obtain

$$Ind_f(total) \approx -1.$$

Thus, the portion of the chain adjacent to the tails that were removed also appears to support (at least one) kinky structure. But the experimental data are not very precise for determining the folding index structure. It should be reminded that the experimental structure of protein A has been determined by NMR as an ensemble of conformations,[33] which makes the folding index analysis unprecise.

B. UNRES analysis of kinks in the backbone of protein A

We have made extensive simulations using the UNRES energy function to study the folding patterns of protein A. In the UNRES effective free-energy function, the effects of water are taken into account implicitly; they are mainly included in the potential of mean force of side chain–side chain interactions.[24] To eliminate noise as much as possible, we analyzed trajectories simulated at T = 250 K; this value of temperature was chosen as a compromise between reasonably fast folding and small noise, after analysis of folding pathways at T = 150 K, 240 K, 250 K, 260 K, 300 K, and 310 K. Although the selected simulation temperature is low, the trajectories simulated at physiological temperature are found to be qualitatively similar to those at lower temperatures except that the folding process takes longer. In particular, we have found that various short duration oscillations and random thermal fluctuations affect only the small-scale ruggedness of the energy landscape, with only very little if any relevance to the folding process *per se*.

The qualitative features of the physical phenomena that we describe in Secs. III B 1 and III B 2 are largely UNRES temperature independent. Consequently we expect that our observations capture the essential aspects of the folding process, over a wide range of solvent environments. A movie has been attached as a supplementary material;[64] it shows both the evolution of the (ungauged) backbone angles and the corresponding three-dimensional C^{α} structure.

1. Third kink

We start our analysis from the third kink which is located at the Gln33–Ser42 segment. We use the conceptual analogy, summarized in Figures 6 and 7, between the profile of the kink and a right-handed-α-helix-loop-right-handed-α-helix supersecondary structure. Accordingly, we are interested in studying how the kink, that describes the loop by interpolating between the two pertinent local minima (a and b in Figure 6), emerges from an initial conformation that is one of the two local minima.

In the present case, a conformation in one of the two local minima corresponds to helical geometry. Consequently, as an initial conformation, we consider the segment Gln33–Ser42 in the right-handed α-helix conformation. We inquire how this becomes deformed into the right-handed-α-helix-loop-right-handed-α-helix conformation of protein A, *i.e.*, how the kink forms. In Figure 12, we show the initial conformation (left) and the kink structure (right); the latter is taken from the PDB. It should be noted that, instead of a monotonous α-helical conformation, we could have started, alternatively, *e.g.*, from a monotonous β-strand or polyproline-II conformation. At the level of the kinks, these latter two possible starting conformations correspond to uniform values of the bond angles which are *different* from a and b, respectively, using the analogy in Figure 6. This would cause initial oscillations and inhomogeneities around the corresponding values a and b. These are local fluctuations that are equally accounted for by thermal noise and are not directly relevant to the kink formation. A change in starting conformation introduces only some transient initial fluctuations around the minimal energy conformations, as shown schematically in Figure 13.

In our extensive UNRES simulations we have found that, typically, the transition between the two conformations in Figure 12 takes place during a very short time period. In Figure 14, it is shown how the free energy of the Gln33–Ser42 segment, computed by using the UNRES effective energy function, which has the sense of a free energy,[28] changes when the transition takes place. The red horizontal dashed lines in this figure correspond to the average UNRES energy

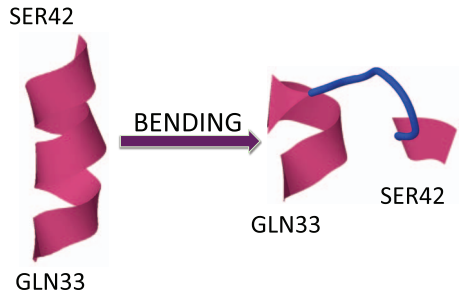

FIG. 12. The initial and final conformations for the third loop between Gln33 and Ser42. The initial conformation (right-handed α-helix) is like minimum a or b in Figure 6, and the final conformation (third loop) is like the kink that interpolates between a and b, in Figure 6. See the profile of bond angles γ_i in Figure 9.

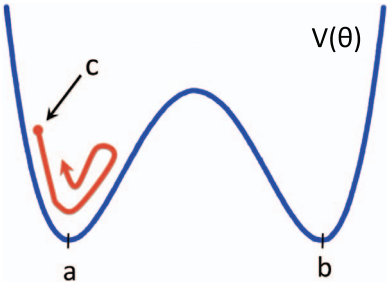

FIG. 13. The initial conformation in Figure 12 is a local minimum conformation while the kink, *i.e.*, loop, forms between two such local minima (*a* and *b*). If another initial conformation is chosen, for example, polyproline-II, these correspond to unstable states such as conformation *c* shown in the figure. This will cause initial conformation-specific embryonic fluctuations around the local minimum. But, already during the very early stages of the folding process, these random fluctuations become mingled with thermal fluctuations and lose their relevance in guiding the folding process. In specifying the initial conformations in our simulations, we try to minimize transient random effects.

averaged over "before" and "after" energy jump (from snapshot 1500 to snapshot 2000 and from snapshot 2001 to snapshot 3200, respectively). It can be seen that the free energy over the putative kink region increases by about 7 kcal/mol, when the kink forms. Because the UNRES energy of the chain decreases during the progress of simulations, the unfavorable free-energy change of 7 kcal/mol, that we observe when the kink forms and the right-handed α-helix breaks to form a right-handed α-helical hairpin, must be compensated by long-range hydrophobic interactions between the side chains of the two α-helices adjacent to the segment that turns into a loop; however, the free energy increases by 7 kcal/mol before the contacts are formed. The 7 kcal/mol value can thus be considered the free energy of kink formation. It can be noted that 7 kcal/mol is very close to the Gibbs free energy that is released by cleaving a phosphate (Pi) unit from adenosine triphosphate (ATP) at 1M concentration.[55] The coupling of ATP hydrolysis to a change of protein conformations is observed in molecular motors:[56]

$$\mathrm{ATP} + \mathrm{H_2O} \rightarrow \mathrm{ADP} + \mathrm{P_i}; \quad \Delta G \approx -7.3\,\mathrm{kcal/mol}.$$

In a future investigation, we propose to clarify whether a connection between kink formation and ATP hydrolysis actually exists.

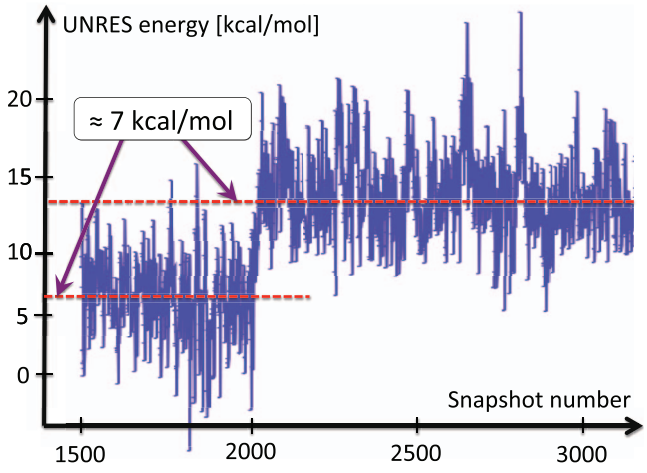

FIG. 14. The UNRES energy change during the formation of the second loop (3rd kink) of protein A, in a generic UNRES simulation. The energy needed to excite the kink is around 7 kcal/mol. The kink formation takes place very rapidly, during a small number of UNRES steps.

2. First and second kinks

As follows from Figures 9 and 11, the first and second kinks are located very close to each other, namely, at Leu20–Pro21 and at Asn24–Glu25, respectively; these will hereafter be referred to as kink 1 and kink 2, respectively. As follows from Figure 11, these two kinks have opposite contributions to the folding index; the first is oriented counterclockwise, while the second is oriented clockwise. It was found from UNRES simulations that either kink 1 or kink 2 can be formed first. The other kink then emerges close to the first one, and slowly drifts away. Moreover, during the initial formation stage, these kinks may form and then again disappear before they become stabilized. The slow speed of the separation suggests that there is a substantial Peierls-Nabarro barrier[57,58] for the kinks to move. It should also be noted that kink 3 is practically stationary along the backbone, which is presumably due to a Peierls-Nabarro barrier. On the other hand, kinks 1 and 2 fluctuate substantially; in particular their shape and their mutual distances oscillate, even at very low temperatures. These fluctuations are visualized in Figure 15, where diagrams of the kinks in the stereographically projected (θ_i, γ_i) plane are shown. The changes in the structure following kink formation are shown in Figure 16.

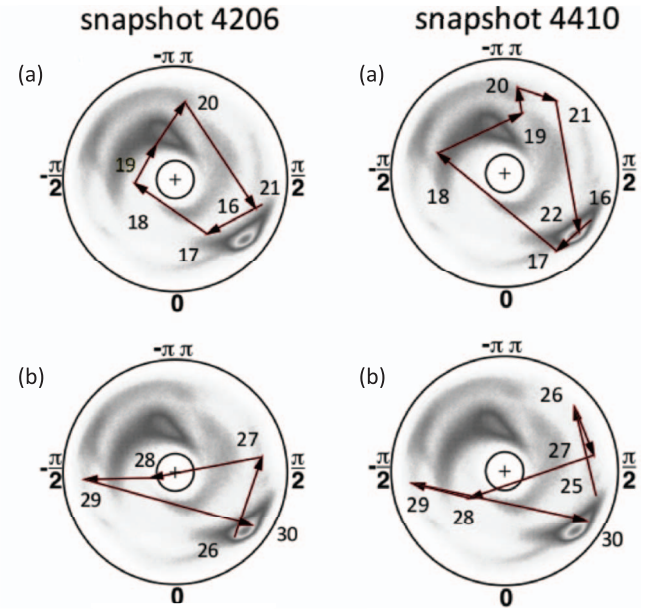

FIG. 15. The trajectories of kink 1 (a) and kink 2 (b), drawn on the stereographically projected (θ_i, γ_i) plane, at two different snapshots in the same simulation. Both trajectories of (a) start at site Glu16. Snapshot 4206 ends at Pro21 and snapshot 4410 ends at Asn22. Trajectories of (b) both end at Gly30; in snapshot 4206, it starts at site Glu26 and in snapshot 4410 at site Glu25. The snapshot values are shown only to indicate that the time difference is very short, and the fluctuations are rapid. A more precise determination of the time difference is not meaningful.

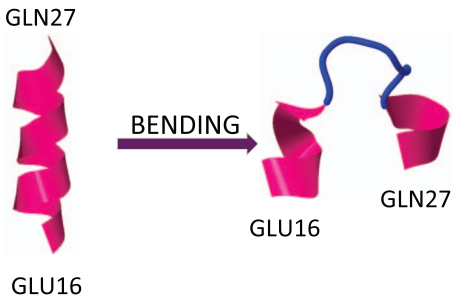

FIG. 16. The initial and final conformations for the loop between Glu16 and Gln27. The initial conformation (right-handed α-helix) is like minimum *a* or *b* in Figure 6, and the final conformation is like a pair of kinks that each interpolate between *a* and *b*, as a kink pair would in Figure 6. See the profile of bond angles γ_i in Figure 9(b).

The kink pairs depicted in Figure 15 both start at the same site, namely Glu16. But at snapshot 4206(a), kink 1 ends one site earlier, *i.e.*, it is shorter. At snapshot 4410(a), the first kink has become extended by one site, towards kink 2. Similarly, the two kinks of pair 2 both end at Gly30. But the second kink at 4410(b) starts one site earlier than the first kink at 4206(b).

It should be noted that the placement of kink 1 at snapshot 4206(a) compares well with the corresponding kink in 1BDD, shown in Figure 9(a); there, the first kink extends between sites 17 and 21. However, the orientation is different: In Figure 9(a) the kink rotates counterclockwise, while in Figure 15(a) it rotates clockwise. Both kinks in Figure 15 are moved away from the N terminus in comparison to the 1BDD conformation. In Figure 15, these kinks both extend to site 30, while in Figure 9(b), kink 1 terminates at site 26. Both kinks 1 and 2 in Figure 15 are also oriented counterclockwise, while in the experimental 1BDD structure the orientation is opposite, *i.e.*, clockwise.

In Figure 17(a), the variation of the UNRES energy of the Asn22–Ile32 segment upon formation of the first kink in a typical UNRES simulation is shown. The visible steps, in which the energy changes by around 7 kcal/mol, corresponds to creation and annihilation of the first kink, which can take place a few times in a typical run before the loop settles down. The smaller changes are due to the kink drifting (partially) outside the window, towards the first kink. This can be seen in Figure 17(b), in which the energy is computed over the sites that separate these two kinks. The variation in the average energy in Figures 17(a) and 17(b) is relatively small, and clearly slower than during the process of kink formation.

In Figure 18, the evolution of the average energy of kink 2 (between Glu16 and Glu27), over a longer period of time than that covered by Figure 17, is shown. An initial formation of a kink pair near the eventual location of the second kink can be observed. The first kink then drifts towards the N-terminus, with stabilization of the second kink towards its thermodynamic equilibrium with energy again about 7 kcal/mol. Finally, in Figure 19, a typical example of a simulation is shown, in which the first kink emerges and stabilizes towards the equilibrium conformation, with energy again about 7 kcal/mol. The energy is computed over a very narrow segment that covers the kink, and the second kink forms outside of the segment in this particular example.

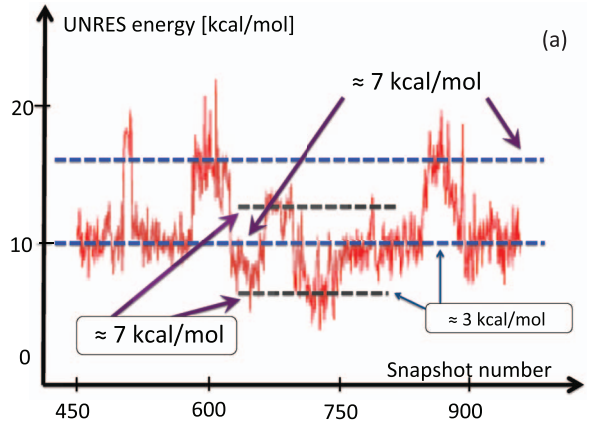

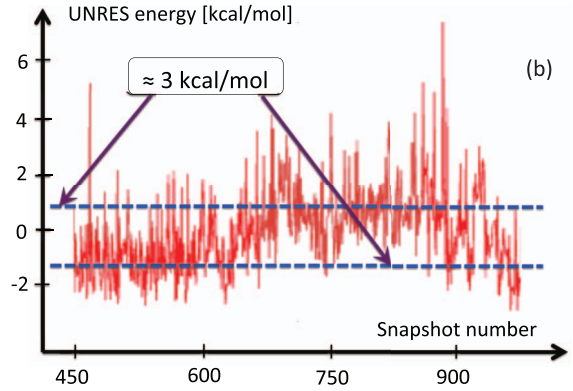

FIG. 17. (a) Energy change during formation of the second kink (sites Asn22-Ile32) of protein A in a generic UNRES simulation. The fluctuations in the average value of energy are consistently around 7 kcal/mol. The kink formation takes place very rapidly during a small number of UNRES steps. Between steps ≈ 620 and 800, the second kink drifts towards the first kink, causing the energy to drop on average of about 3 kcal/mol. (b) The average energy between the first two kinks increases by an amount that is comparable to the decrease in average energy in (a). The change is due to oscillation in the distance between the two kinks; the second one drifts towards the first one, causing the energy to increase.

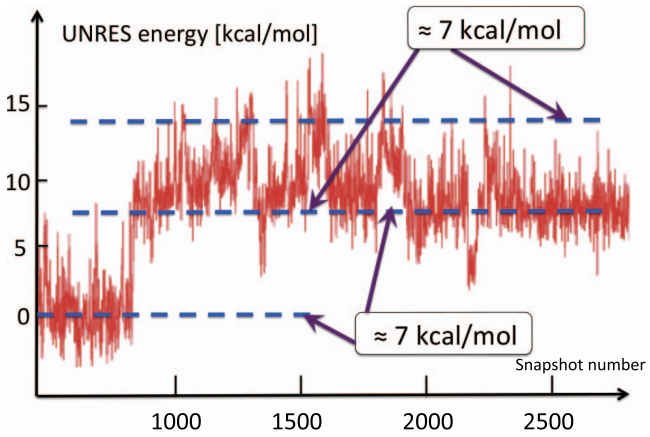

FIG. 18. The energy change between the initial and final conformations for the loop between Glu16 and Gln27 (the region of the first and the second kink). The initial conformation (right-handed α-helix) is like minimum *a* or *b* in Figure 6, and the final conformation is like a pair of kinks that each interpolate between *a* and *b*, as in Figure 6. See the profile of the virtual-bond angles θ_i in Figure 9(b).

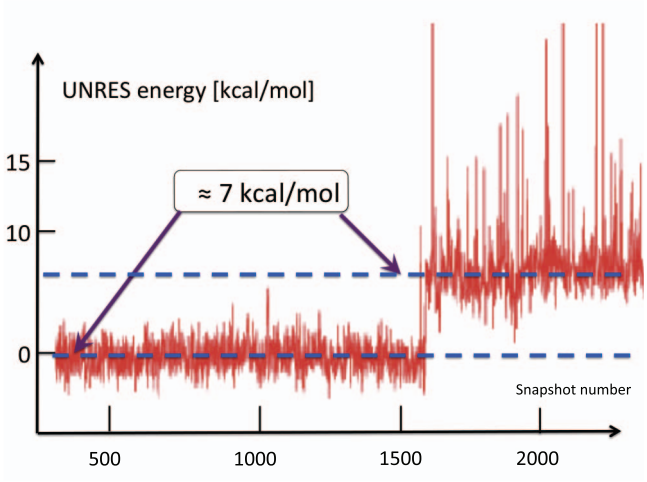

FIG. 19. The energy change between the initial and final conformations for the loop between Glu16 and Leu20 (the region of the first kink). The initial conformation (right-handed α-helix) is like minimum a or b in Figure 6, and the final conformation is like a pair of kinks that each interpolate between a and b, as in Figure 6. See the profile of the virtual-bond angles θ_i in Figure 9(b).

C. UNRES analysis of side-chains in protein A

According to Figure 5, the $C^\alpha \cdots C^\beta$ vector **s** [Eq. (15)] is strongly slaved to the backbone geometry. Conversely, it may be argued that the backbone is slaved to the side chains. In fact, there appears to be a duality between the backbone and the side chains, to the extent that the coordinates of either of these two types of sites may be utilized to describe the folding. Here, the kink (loop) formation is discussed in terms of side-chain geometry, because it provides some visual advantages over the backbone-based description.

It should be noted that the DNLS equation has a natural interpretation in terms of a (magnetic) spin-chain: The variable γ_i can be identified as the order parameter for magnetization in a two-state ferromagnet.[59] Positive values of γ_i describe a "spin-up" state, while negative values correspond to a "spin-down" state; the absolute value characterizes the strength of the magnetization. The kink, Eq. (21), can be interpreted as the continuum-chain limit of a (magnetic) Bloch domain wall[60] that interpolates between the two (ferromagnetic) spin states. See Figure 20.

Using an energy-based procedure,[61,62] we converted the coarse-grained trajectories to all-atom trajectories and then computed the unit $C^\alpha \cdots C^\beta$ vectors **s** from Eq. (15). The

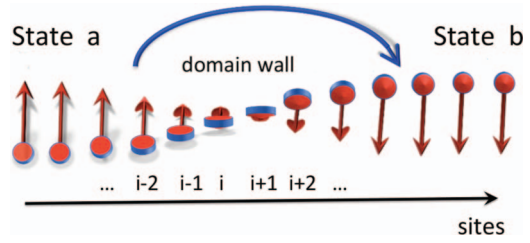

FIG. 20. The kink in Figure 6 is the boundary between the two minima a and b. It can be interpreted as a continuum limit of a magnetic Bloch-type domain wall that interpolates between spin-up state (a) and spin-down state (b). Here, we show, as an example, the Bloch wall in the transversal O(2) spin model.

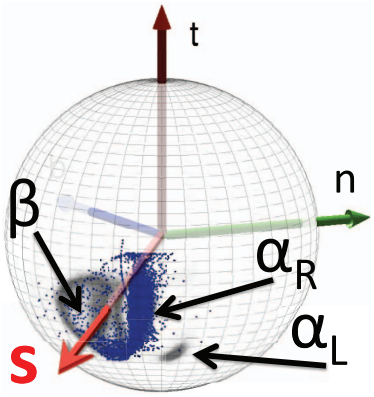

FIG. 21. Statistical distribution of C^β directions during a generic UNRES collapse simulation, in the backbone Frenet frames. The vectors **s** of Eq. (15) are near parallel to their average values, during the entire collapse transition.

folding pathways were subsequently analyzed in terms of the vectors **s**. A protein molecule can then be interpreted as a one-dimensional spin chain akin that in Figure 20, with the sites identified as the C^α atoms and the vectors **s** with Eq. (15). Since these vectors can point in any direction in $\mathbb{R}^3$, this is a variant of the O(3) Heisenberg spin chain[59] rather than a two-state Ising spin chain.[59]

We have investigated in detail how the direction of the vector **s** of Eq. (15) evolves during the simulated formation of the tertiary structure of protein A. A typical result is shown in Figure 21. The initial conformation in this particular simulation is a linear right-handed α-helix. We find that during the entire collapse simulation, the vectors **s** of Eq. (15) along the backbone are very strongly coupled to the backbone geometry. The deviations from the background shown in Figure 5 (grey area in Figure 21) are minuscule, during the entire helix-packing transition. This confirms that the direction vectors **s** of Eq. (15) can indeed be used to describe the transformation of the full-α-helical conformation of protein A into a native-like conformation in UNRES simulations.

As an illustrative example of our observations, in Figure 22 the bond and torsion angles (θ and γ) of kink 3 (the second loop) are described, as they appear during a generic UNRES run.

To describe kink formation in terms of the change of the orientation of the C^β atoms, the dihedral angles η defined by $C_i^\beta \cdots C_i^\alpha \cdots C_{i+1}^\alpha \cdots C_{i+1}^\beta$ are utilized. These angles are computed as those between the consecutive **u** vectors, each being computed from the respective vector **s** by orthogonalization to the transversal **t** vectors, as defined by Eqs. (22) and (23):

$$\mathbf{u}_i = \frac{\mathbf{s}_i - (\mathbf{s}_i \cdot \mathbf{t}_i)\,\mathbf{t}_i}{1 - (\mathbf{s}_i \cdot \mathbf{t}_i)^2}, \tag{22}$$

$$\eta_{i,i+1} = \mathrm{sgn}[\mathbf{t}_i \cdot (\mathbf{t}_i \times \mathbf{t}_{i+1})]\ \arccos(\mathbf{u}_i \cdot \mathbf{u}_{i+1}). \tag{23}$$

The dihedral angle η is the side-chain $O(2)$ order parameter that will be utilized. For regular structures, the value of η is constant along the chain; for example, for a right-handed α-helix, $\eta \approx 0.75$ (rad) and, for a β-strand, $\eta \approx \pi$ (rad). For a single kink, the values of the angle η interpolate between

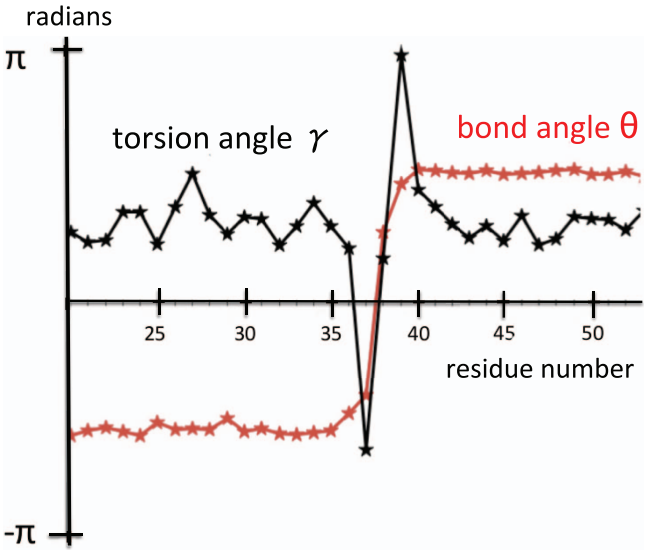

FIG. 22. Values of θ and γ of a generic conformation during an UNRES simulation, corresponding to the third kink (second loop) of 1BDD.

those that correspond to the adjacent regular structures, much as in Figure 6.

In Figure 23(a), the vectors $\mathbf{s}_i$ are displayed along one turn of the right-handed α-helix, and in Figure 23(b) the definition of the angle η in terms of the vectors $\mathbf{s}$ of Eq. (15) is illustrated.

In terms of the side-chain vectors, the loop region, the backbone angles of which are plotted in Figure 22, has the structures shown in Figures 24 and 25.

In these figures, the side-chain orientations of the vectors of Eq. (15) between two consecutive sites i and $i+1$, in the projection to the plane which is normal to the tangent vector $\mathbf{t}_i$ that connects them are compared. In both the experimental 1BDD structure and the UNRES simulated structure, the side chains rotate once in the clockwise direction as the kink is traversed starting from the Asp37–Asp38 bond, like a Bloch domain wall in a magnetic spin chain. The previous bond (Lys36–Asp37) is in the α-helical state shown in Figure 23 for both experimental and simulated structures. In the UNRES-simulated structures, the side-chain rotation reaches back to the α-helical position at the bond between

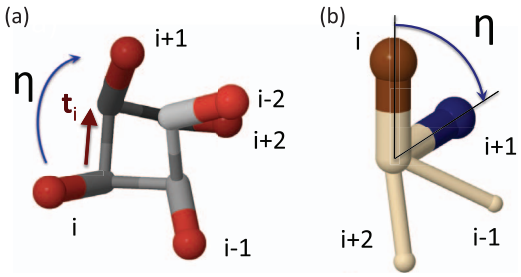

FIG. 23. (a) A right-handed α-helix with the vectors $\mathbf{s}$ [Eq. (15)], viewed along the $C^{\alpha}\cdots C^{\beta}$ axis. (b) Two consecutive vectors $\mathbf{s}$ [Eq. (15)] along the right-handed α-helix, viewed along the tangent vector $\mathbf{t}_i$ that connects the successive C^{α} atoms. The angle of their projection onto the plane, which is normal to the vector $\mathbf{t}_i$ is given by Eq. (23). The top of the vector $\mathbf{s}_{i+1}$ is colored blue in (b) to distinguish it from the top of the vector $\mathbf{s}_i$.

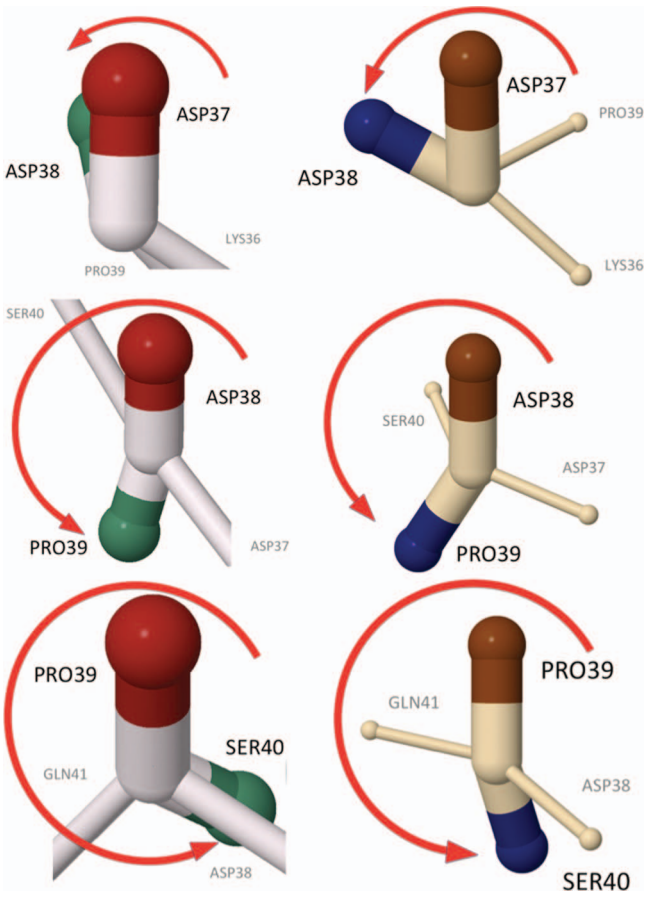

FIG. 24. The side-chain structure of the second loop in the experimental structure of 1BDD (left) and of the UNRES kink (right) (whose profile is shown in Figure 22). The figures show the evolution of the relative torsional angles [Eq. (23)], along the residue number. In both the experimental 1BDD structure and the UNRES kink, the angles η prior to the Asp37-Asp38 bonds are in the right-handed α-helical position, as shown in Figure 23(b).

Gln41 and Ser42, while in 1BDD the kink terminates in the α-helical position between Ser42 and Ala43. In both cases, the loop can be clearly interpreted as a Bloch domain wall akin to the one shown in Figure 20.

In Figure 26, the time evolution of the angles of Eqs. (23) during a generic UNRES run is shown for the six bonds between Asp37 and Ala43. In the initial conformation, the angles η are all close to the right-handed α-helical values (0.75 rad). It can be observed that the transitions are abrupt, taking place during a very small number of UNRES/MD steps; it should be noted that strong fluctuations between values around $\pm\pi$, that are seen in each of the figures, are due to the 2π periodicity of the angular variable, whose fundamental range is $\eta \in [-\pi, \pi)$. It can also be noted that there are only very few clearly identifiable equilibrium values for η, in decreasing order

$$\langle\eta\rangle \approx \pi,\ 2\,,\ 1,\ -1,\ -2,\quad (\mathrm{mod}\ 2\pi).$$

This is consistent with the kink structure of the side chain-side chain interaction potential; it appears to have the functional form akin to the torsion angle in the expression for the conformational energy

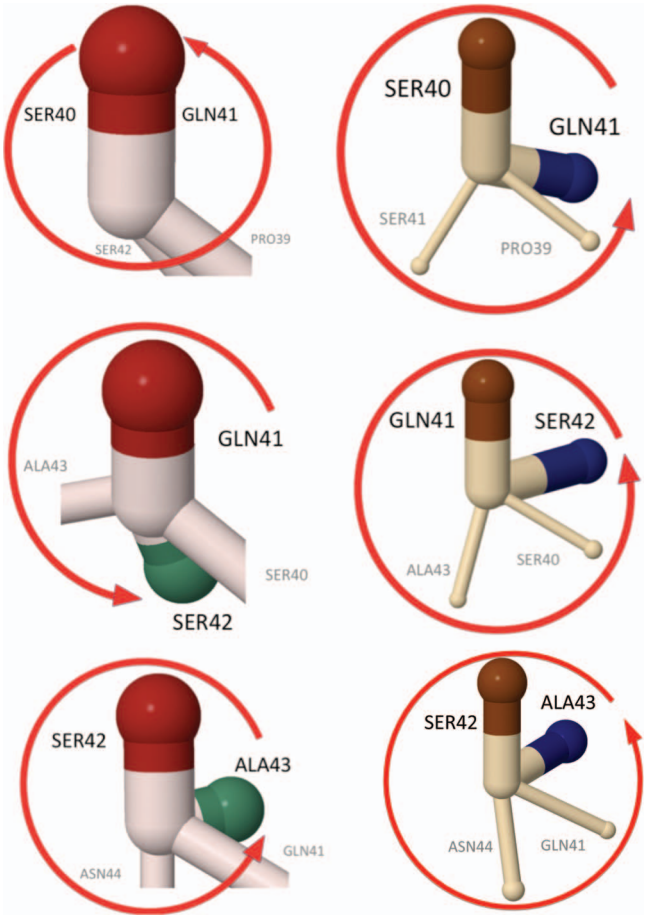

FIG. 25. Continuation of Figure 24, along the 1BDD and UNRES kink backbones. In the UNRES kink, the bond between Gln41 and Ser42 returns back to the initial α-helical position, and in 1BDD, the kink is one step longer. The green and blue colors are used to distinguish side chains that belong to consecutive residues.

$$V(\eta_{i,i+1}) \sim \sum_a V_a \cos(\eta_{i,i+1} - \eta_a),$$

where V_a is a torsional constant, and the loop is a kink conformation that forms the boundary between two neighboring minima of the potential.

D. UNRES analysis of kink dynamics

We now turn to describe the mechanism that we have identified as the cause of the kink formation, *i.e.*, the transition in which a local oscillation as in Figure 13 becomes converted into a conformation shown in Figure 12. For this transition to take place, the local oscillations such as those portrayed in Figure 13, must exceed the threshold energy that enables them to overcome the potential barrier between the minima a and b. We have confirmed that these oscillations have a thermal origin. For example, in our UNRES simulations at very low temperatures (100 K), we observe that it takes a long time to form a loop from an initial α-helical conformation (data not shown). This is due to the presence of the energy barrier of about 7 kcal/mol for the kinks to form, and at sufficiently low temperatures the thermal oscillations are unable to exceed this threshold value.

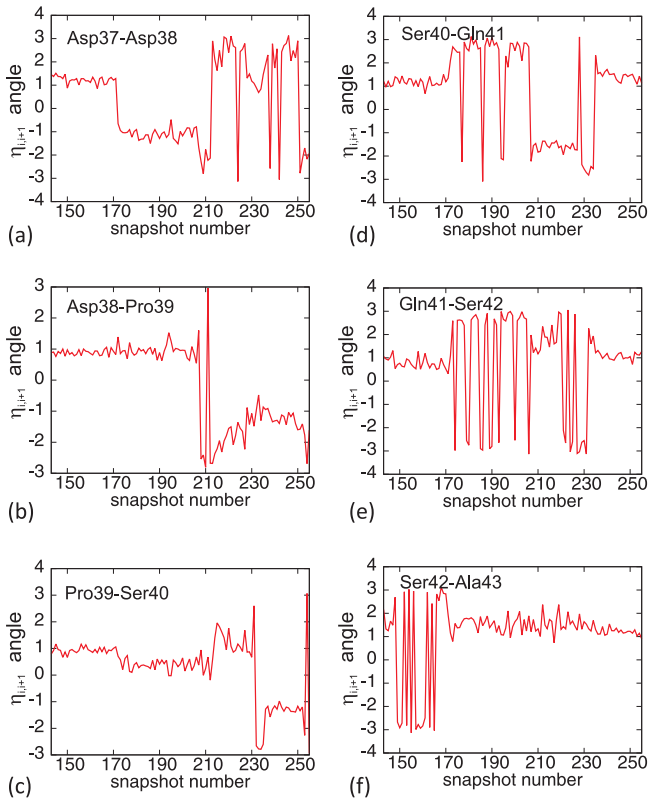

FIG. 26. ((a)–(f)) Time evolution of the angles $\eta_{i,i+1}$ of Eq. (23) during a generic UNRES simulation, over the location of the third kink.

1. Backbone lattice oscillations

The thermal oscillations cause localized bending and twisting deformations in an α-helical segment. The α-helical structure in a protein is stabilized by longitudinal hydrogen bonds, and there are three parallel channels that run along the helix. Each of the channels has the composition $\cdots$H-N-C=O$\cdots$H-N-C=O$\cdots$H-N-C=O$\cdots$. The three channels can vibrate due to the C=O stretching (amide I vibrations).

It should be noted that, although the whole channel of H-N-C=O groups is treated as a single interaction site in UNRES, and their atoms are not present explicitly, the internal motions of the peptide groups are included implicitly in the UNRES energy function through the second- and higher-order terms of the cumulant expansion for the potential of mean force (restricted free energy) of polypeptide chains.[26] The ensuing oscillations are quasiparticles that interact with the phonons of the longitudinal displacements of the amino acids. The three channels are also directly coupled to each other, by nearest neighbor dipole-dipole interactions. There are three different channels and, in addition to a longitudinal compression, a generic backbone C^α-lattice displacement also involves distortions such as bending and twisting of the right-handed α-helix.

We have observed that, in UNRES simulations, wave-like distortions of the C^α-lattice are constantly present. The waves that we observe travel along the protein chain and with a very high speed. The time it takes for a typical distortion to traverse the entire backbone is no more than a few hundreds of picoseconds, in UNRES time. In Figure 27, we show as an

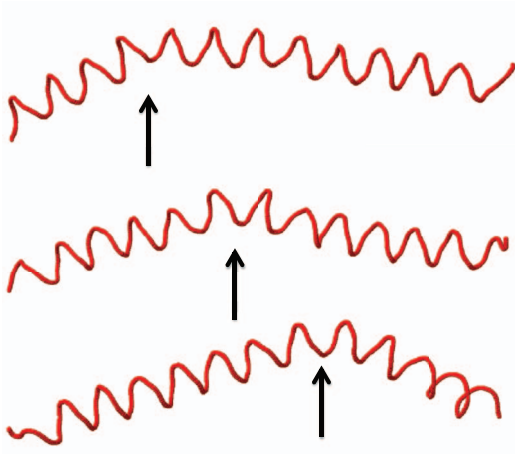

FIG. 27. An example of a bending deformation that proceeds along an initial α-helical protein A conformation.

example how a thermally excited bending deformation proceeds along a protein A chain in an α-helical initial conformation. In Figure 28, we show an example of a twisting deformation that we have observed. On average, the deformation propagates 6.2 residues (forward or backward) per snapshot (1000 time steps at 4.89 fs UNRES time), which gives 0.030 ns UNRES propagation time from residue to residue. However, because of elimination of fast-moving degrees of freedom, the UNRES time scale is by about 3 orders of magnitude faster compared to the all-atom time scale[23,53] and, therefore, the deformation-propagation time can be estimated to be about 30 ns. This value is by about an order of magnitude greater than the rate of helix propagation in α-helical peptides;[63] however, our simulations were run at a low temperature of $T = 250$ K to reduce the random motion that could disturb the analysis of the kink structure.

In our interpretation, the lattice deformations that we observe are propagating phonon waves due to amide vibrations. Since UNRES is a reduced atom model, we are not able to fully identify their detailed character. For a detailed investigation of the deformations that we observe, all-atom simulations would be necessary.

A movie that displays the propagation of the deformation of the virtual-bond and virtual-bond-dihedral angles during the course of simulation is included in the supplementary material.[64]

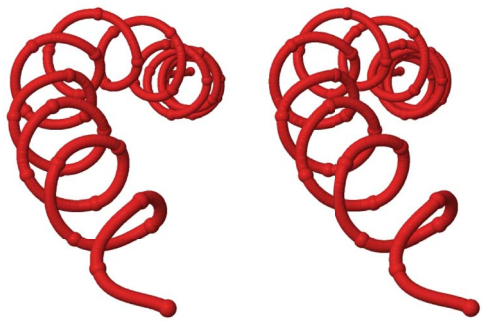

FIG. 28. Stereoview of an example of a twisting deformation along an initial α-helical protein A conformation.

Finally, it is observed that the residues in the loop regions are especially prone to hopping from one minimum of the potential of mean force to the other one. Based on the discussion presented in Sec. III C, it can be concluded that interactions between the neighboring side chains can trigger kink formation, propagating it as a spin wave.

E. UNRES, principal component analysis

Principal component analysis, a covariance-matrix-based mathematical technique, is an effective method for extracting important motions from molecular dynamics trajectories.[65–68] PCA rotates the Cartesian or internal coordinate space to a new space with new coordinates, PCs, a few of which are sufficient to describe a large part of the fluctuations of a protein. Here, structural fluctuations of θ and γ angles [mean-square-fluctuations (MSF)] can be decomposed into collective modes by PCA.[44,66–68] The modes have "frequencies" and directions corresponding to the eigenvalues and eigenvectors of the covariance matrix. The modes with the largest eigenvalues (λ_i) correspond to the modes which contribute the most to the structural fluctuations of the protein. The contribution of each angle (θ_n and γ_n) to a mode i is called the influence, $\nu_{i,n}$.

The kinks describe loops, which are flexible, and consequently the kinks certainly correspond to principal modes. But the exact correspondence is not known. In particular, one might inquire whether PCA is sensitive enough for identifying, and possibly analyzing, kinks in the background of generic motions? A good demonstration of this is the movie (see the supplementary material[64]), which illustrates the evolution of the backbone angles. The peaks which appeared along the backbone angles in the course of time coincide with the peaks that appeared in the principal modes calculated at the corresponding time intervals.

MD trajectories of protein A were analyzed by PCA. The results are displayed in Figure 29 as the contributions of the two main principal modes (with the largest eigenvalues) to the MSF along the θ and γ angles for different trajectory windows. It can be seen that the peaks in the contributions appear *exactly* in the regions where the kinks are located. There are three peaks in the initial time window (Figures 29(a) and 29(b)), the middle of which reflects the traveling kink structure, which is visualized in Figure 27. After 4890 ps UNRES time (Figures 29(c) and 29(d)), only two peaks appear which correspond to the stabilization of a folded structure. The bands in Figure 29, corresponding to the contribution from the variation of the virtual-bond angles θ, are unimodal, while those corresponding to the contributions from the γ angles have finer structure; this is similar to the shapes of the kink profiles in the θ and γ angles of the experimental 1BDD structure (Figure 9).

It should be noted that MD simulations, in the presented work, were started from the full right-handed α-helix. The principal modes do not exhibit any peaks in kink regions until loops form (not shown). This is because the first principal modes capture the largest fluctuations, which do not come from helices. Once loops are formed (consequently the kinks), which are more flexible and characterized with fluctuations

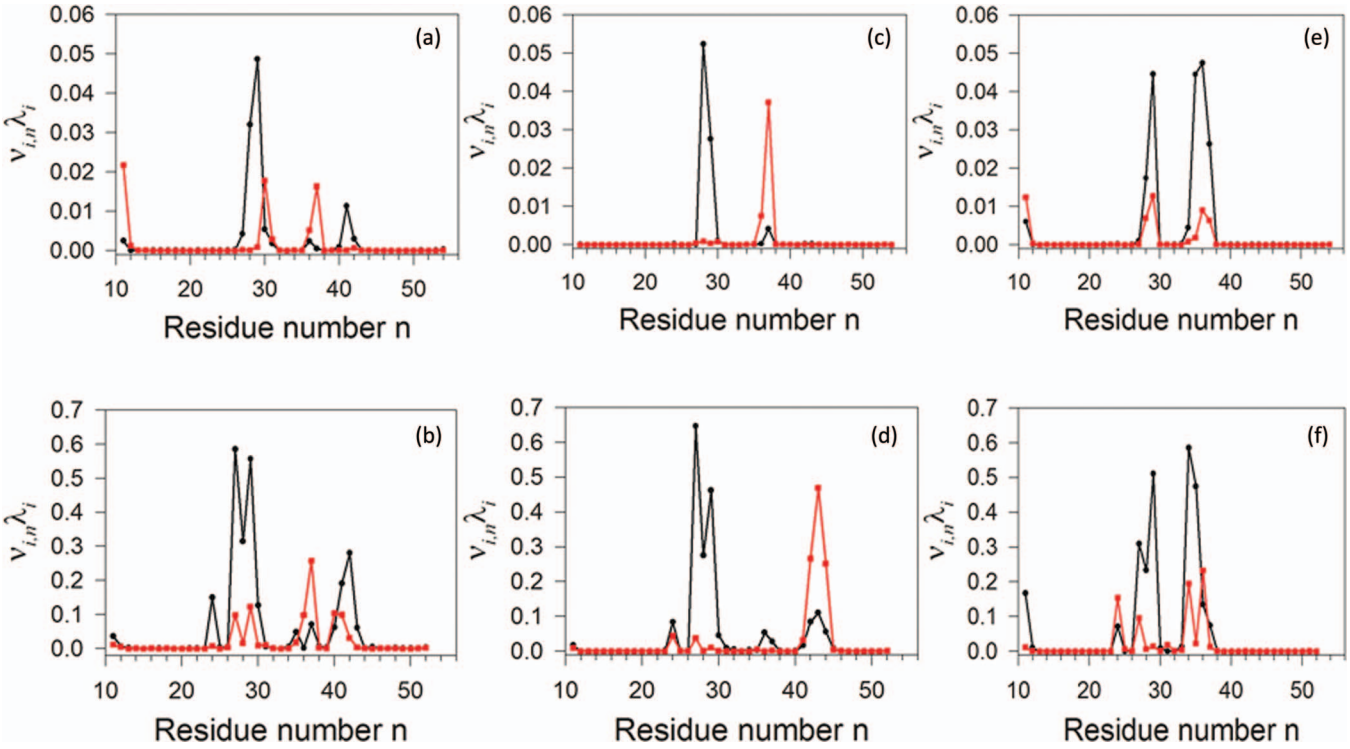

FIG. 29. Contributions ($\nu_{i,n}$, λ_i) of principal mode 1 (black) and mode 2 (red) to the mean-square fluctuations along the θ ((a), (c), and (e)) and γ ((b), (d), and (f)) angles, respectively, in the time windows from 0 to 4.89 ns ((a) and (b)), 4.89 to 9.78 ns ((c) and (d)), and from 9.78 to 14.67 ns ((e) and (f)).

greater than those in the helices, the peaks start to appear in principal modes in kink regions.

It is remarkable that the shapes of the contributions of the principal modes to mean square fluctuations along θ and γ angles resemble those of the squares of the derivatives of the kink profiles. This feature probably arises since the contributions plotted in Figure 29 are variances of the respective θ or γ angles along a given principal component. Following error propagation rules, the variance of a composite quantity is proportional to the square of the derivative of a quantity. Therefore, the more an angle varies along the chain, the greater are its fluctuations.

IV. CONCLUSIONS

The folding pathway of the N-terminal segment of the B-domain of staphylococcal protein A has been simulated in this work with the coarse-grained UNRES force field.[24–28,30–32] The analysis demonstrates that the description of protein structure in terms of kinks of the DNLS equation proposed in our earlier work[6,7,9] can be applied to the description of protein folding pathways and energetics. Intuitively, this feature of protein structure and dynamics is seen to result from the approximate bimodal character of the local potential of mean force of polypeptide chains in backbone virtual-bond angles θ (Figure 6). This can be seen both in the statistic of the PDB (Figure 4; see also Ref. 25) and from the potential of mean force calculated from *ab initio* energy surfaces of terminally blocked amino-acid residues.[69]

The present kink structure is, in particular, useful in representing chain-reversal structure which seems to be crucial in initiating nucleation sites, which then enable the formation of long-range contacts between side chains.[70,71] For protein A, the kinks are located in the regions between residues Glu16-Asn22, Leu20-Asn29, and Gln33-Asn44, respectively. The trajectories that were analyzed in this work had been started from a full-α-helical conformation but this starting point had been selected to focus the observation on loop formation instead of on the formation of α-helices from random structure. Moreover, transitions from a long right-handed α helix to a helical hairpin structure is part of functionally important motions of many proteins; e.g., the transition from an open to a closed (substrate-binding) conformation of Hsp70 chaperones;[72–74] it also constitutes a part of folding of many proteins such as, e.g., the engrailed homeodomain.[75]

Kink analysis enables us to realize the importance of local interactions, specifically the bimodal character of the potential of mean force in virtual-bond angles θ, as the driving force of folding. The Landau Hamiltonian used in this study and in the studies reported in our earlier work[6–10,48] does not contain any long-range terms. Still, it was usable to simulate folding pathways in our earlier studies[10] in a Gō-like manner, using kink parameters derived from the experimental structure of the protein under study. In this regard, the kinks can provide a prediction of local collective motions without MD simulations, while PCA requires MD simulations for this. Moreover, we learned from our current study that the bimodal character of the potentials in the virtual-bond angles θ makes the system jump from state to state, causing conformational transitions.

A remarkable observation made during this study is that the creation of a kink in a full-α-helical protein segment

consistently involves a *local* free energy increase of about 7 kcal/mol. Surprisingly, this is a value which is very close to the dissociation of a phosphate residue from ATP. However, it remains to be clarified in future work, whether the observation, that the energy for the initiation of helix bending in protein A is equal to the elementary energy supply from ATP hydrolysis, is accidental.

Even though bimodality of the potential of mean force in backbone virtual-bond valence angles characterizes all amino-acid residues, some of them are more prone to change their local conformational state. The analysis presented in Sec. III C suggests that the interactions between neighboring side chains or the side chains and adjacent backbone sites trigger the jump from one local minimum to another one. This process is similar to the formation of a Bloch domain wall in magnetic spin chains. It should be noted that, apart from kink initiation, we also observe very fast-moving wave-like phonon propagation along the chain (Figure 27). For a detailed investigation of these wave-like structures, all-atom simulations should be performed.

Finally, a principal-component analysis of the folding trajectories of protein A in Sec. III E has shown that the principal modes appear to be clearly correlated with kink formation. As expected, the largest contributions to the most significant principal modes arise from loop regions (Figure 29), and the shapes of the plots of the principal modes along the chain resembles the directional derivative of the solution of the DNLSE (cf. Sec. III E). But the strong correlation observed here between PCA and kink formation is somewhat unexpected. This observation suggests that kinks can be used to describe principal motions of proteins without having to resort to *a posteriori* essential dynamics. This line of research is now being followed in our laboratory.

ACKNOWLEDGMENTS

This work was supported by grants from the National Institutes of Health (GM-14312), the National Science Foundation (MCB10-19767), by the Polish National Science Centre (2012/06/A/ST4/00376), by the Carl Tryggers Stiftelse för Vetenskaplig Forskning, by a CNRS PEPS collaboration grant, by a Qian Ren grant at the Beijing Institute of Technology (BIT), by an Égide—Programme Cai Yuanpei collaboration grant, and by a Région Centre research grant. A.L. thanks the Department of Physics and Astronomy at Uppsala University for hospitality during this collaboration. Computational resources were provided by (a) Argonne Leadership Computing Facility at Argonne National Laboratory, which is supported by the Office of Science of the U.S. Department of Energy under Contract No. DE-AC02-06CH11357, (b) the National Science Foundation (http://www.nics.tennessee.edu/), and by the National Science Foundation through TeraGrid resources provided by the Pittsburgh Supercomputing Center, (c) the Informatics Center of the Metropolitan Academic Network (IC MAN) in Gdańsk, (d) our 624-processor Beowulf cluster at the Baker Laboratory of Chemistry, Cornell University, and (e) our 184-processor Beowulf cluster at the Faculty of Chemistry, University of Gdańsk.

[1] C. A. Orengo, A. D. Michie, S. Jones, D. T. Jones, M. B. Swindells, and J. M. Thornton, Structure **5**, 1093 (1997).
[2] A. G. Murzin, S. E. Brenner, T. Hubbard, and C. Chothia, J. Mol. Biol. **247**, 536 (1995).
[3] S. Rackovsky, Proteins Struct. Funct. Genet. **7**, 378 (1990).
[4] J. Skolnick, A. K. Arakaki, Y. L. Seung, and M. Brylinski, Proc. Natl. Acad. Sci. U.S.A. **106**, 15690 (2009).
[5] L. Holm, C. Ouzounis, C. Sander, G. Tuparev, and G. Vriend, Protein Sci. **1**, 1691 (1992).
[6] M. Chernodub, S. Hu, and A. J. Niemi, Phys. Rev. E **82**, 011916 (2010).
[7] N. Molkenthin, S. Hu, and A. J. Niemi, Phys. Rev. Lett. **106**, 078102 (2011).
[8] S. Hu, A. Krokhotin, A. J. Niemi, and X. Peng, Phys. Rev. E **83**, 041907 (2011).
[9] A. Krokhotin, A. Niemi, and X. Peng, Phys. Rev. E **85**, 031906 (2012).
[10] A. Krokhotin, M. Lundgren, and A. J. Niemi, Phys. Rev. E **86**, 021923 (2012).
[11] In Refs. 6–10 the epithet *topological (dark) soliton* was used, but here *kink* is preferred. This choice highlights that the potential in the DNLS equation displays spontaneous breakdown of a discrete symmetry, and the kink describes the ensuing domain wall; see Refs. 12–16. It should be noted that the kink considered here has no direct relationship with the concept of Davydov's soliton A. S. Davydov, J. Theor. Biol. **66**, 379 (1977): When two kinks collide, their shapes in general change. But when solitons collide, their shapes remain intact.
[12] L. D. Faddeev and L. Takhtajan, *Hamiltonian Methods in the Theory of Solitons* (Springer Verlag, Berlin, 1987).
[13] M. J. Ablowitz, B. Prinardi, and A. Trubatch, *Discrete and Continuous Nonlinear Schrödinger Systems* (Cambridge University Press, Cambridge, 2004).
[14] P. Kevrekidis, *The Discrete Nonlinear Schrödinger Equation: Mathematical Analysis, Numerical Computations and Physical Perspectives* (Springer-Verlag, Berlin, 2009).
[15] N. Manton and P. Sutcliffe, *Topological Solitons* (Cambridge University Press, Cambridge, 2004).
[16] S. Weinberg, *The Quantum Theory of Fields*, Vol. 2 (Cambridge University Press, 1995).
[17] F. C. Bernstein, T. F. Koetzle, G. J. B. Williams, E. F. J. Meyer, M. D. Brice, J. R. Rodgers, O. Kennard, T. Shimanouchi, and M. Tasumi, J. Mol. Biol. **112**, 535 (1977).
[18] M. Khalili, A. Liwo, F. Rakowski, P. Grochowski, and H. Scheraga, J. Phys. Chem. B **109**, 13785 (2005).
[19] D. E. Shaw, M. M. Deneroff, R. O. Dror, J. S. Kuskin, R. H. Larson, J. K. Salmon, C. Young, B. Batson, K. J. Bowers, J. C. Chao, M. P. Eastwood, J. Gagliardo, J. P. Grossman, C. R. Ho, D. J. Ierardi, I. Kolossváry, J. L. Klepeis, T. Layman, C. McLeavey, M. A. Moraes, R. Mueller, E. C. Priest, Y. Shan, J. Spengler, M. Theobald, B. Towles, and S. C. Wang, Commun. ACM **51**, 91 (2008).
[20] M. S. Friedrichs, P. Eastman, V. Vaidyanathan, M. Houston, S. Legrand, A. L. Beberg, D. L. Ensign, C. M. Bruns, and V. S. Pande, J. Comput. Chem. **30**, 864 (2009).
[21] V. S. Pande, I. Baker, J. Chapman, S. Elmer, S. Kaliq, S. M. Larson, Y. M. Rhee, M. R. Shirts, C. D. Snow, E. J. Sorin, and B. Zagrovic, Biopolymers **68**, 91 (2003).
[22] K. Lindorff-Larsen, N. Trbovic, P. Maragakis, S. Piana, and D. E. Shaw, J. Am. Chem. Soc. **134**, 3787 (2012).
[23] A. Liwo, M. Khalili, and H. A. Scheraga, Proc. Natl. Acad. Sci. U.S.A. **102**, 2362 (2005).
[24] A. Liwo, S. Ołdziej, M. R. Pincus, R. J. Wawak, S. Rackovsky, and H. A. Scheraga, J. Comput. Chem. **18**, 849 (1997).
[25] A. Liwo, M. R. Pincus, R. J. Wawak, S. Rackovsky, S. Ołdziej, and H. A. Scheraga, J. Comput. Chem. **18**, 874 (1997).
[26] A. Liwo, C. Czaplewski, J. Pillardy, and H. A. Scheraga, J. Chem. Phys. **115**, 2323 (2001).
[27] A. Liwo, M. Khalili, C. Czaplewski, S. Kalinowski, S. Ołdziej, K. Wachucik, and H. Scheraga, J. Phys. Chem. B **111**, 260 (2007).
[28] A. Liwo, C. Czaplewski, S. Ołdziej, A. V. Rojas, R. Kaźmierkiewicz, M. Makowski, R. K. Murarka, and H. A. Scheraga, in *Coarse-Graining of Condensed Phase and Biomolecular Systems*, edited by G. Voth (CRC Press, 2008), Chap. 8, pp. 107–122.
[29] Y. He, Y. Xiao, A. Liwo, and H. A. Scheraga, J. Comput. Chem. **30**, 2127 (2009).
[30] U. Kozłowska, G. G. Maisuradze, A. Liwo, and H. A. Scheraga, J. Comput. Chem. **31**, 1154 (2010).

[31]A. K. Sieradzan, H. A. Scheraga, and A. Liwo, J. Chem. Theory Comput. **8**, 1334 (2012).
[32]A. K. Sieradzan, U. H. E. Hansmann, H. A. Scheraga, and A. Liwo, J. Chem. Theory Comput. **8**, 4746 (2012).
[33]H. Gouda, H. Torigoe, A. Saito, M. Sato, Y. Arata, and I. Shimada, Biochemistry **31**, 9665 (1992).
[34]Y. W. Bai, A. Karimi, H. J. Dyson, and P. E. Wright, Protein Sci. **6**, 1449 (1997).
[35]G. Dimitriadis, A. Drysdale, J. K. Myers, P. Arora, S. Radford, T. G. Oas, and D. A. Smith, Proc. Natl. Acad. Sci. U.S.A. **101**, 3809 (2004).
[36]S. Sato, T. L. Religa, V. Daggett, and A. R. Fersht, Proc. Natl. Acad. Sci. U.S.A. **101**, 6952 (2004).
[37]A. Kolinski and J. Skolnick, Proteins Struct. Funct. Genet. **18**, 353 (1994).
[38]J. Lee, A. Liwo, and H. A. Scheraga, Proc. Natl. Acad. Sci. U.S.A. **96**, 2025 (1999).
[39]D. O. V. Alonso and V. Daggett, Proc. Natl. Acad. Sci. U.S.A. **97**, 133 (2000).
[40]A. Ghosh, R. Elber, and H. A. Scheraga, Proc. Natl. Acad. Sci. U.S.A. **99**, 10394 (2002).
[41]A. E. García and J. N. Onuchic, Proc. Natl. Acad. Sci. U.S.A. **100**, 13898 (2003).
[42]J. A. Vila, D. R. Ripoll, and H. A. Scheraga, Proc. Natl. Acad. Sci. U.S.A. **100**, 14812 (2003).
[43]M. Khalili, A. Liwo, and H. Scheraga, J. Mol. Biol. **355**, 536 (2006).
[44]G. G. Maisuradze, A. Liwo, and H. A. Scheraga, Phys. Rev. Lett. **102**, 238102 (2009).
[45]G. G. Maisuradze, A. Liwo, S. Ołdziej, and H. Scheraga, J. Am. Chem. Soc. **132**, 9444 (2010).
[46]S. Hu, M. Lundgren, and A. J. Niemi, Phys. Rev. E **83**, 061908 (2011).
[47]M. Lundgren, A. Krokhotin, and A. J. Niemi, Phys. Rev. E **88**, 042709 (2013).
[48]A. Krokhotin, A. Liwo, A. J. Niemi, and H. A. Scheraga, J. Chem. Phys. **137**, 035101 (2012).
[49]B. Widom, J. Chem. Phys. **43**, 3892 (1965).
[50]L. P. Kadanoff, Physics **2**, 263 (1966).
[51]K. Wilson, Phys. Rev. B **4**, 3174 (1971).
[52]M. E. Fisher, Rev. Mod. Phys. **46**, 597 (1974).
[53]M. Khalili, A. Liwo, A. Jagielska, and H. Scheraga, J. Phys. Chem. B **109**, 13798 (2005).
[54]H. J. C. Berendsen, J. P. M. Postma, W. F. van Gunsteren, A. DiNola, and J. R. Haak, J. Chem. Phys. **81**, 3684 (1984).
[55]J. Berg, J. L. Tymoczko, and L. Stryer, *Biochemistry*, 6th ed. (W. H. Freeman, New York, 2007).
[56]N. Thomas and R. A. Thornhill, J. Phys. D: Appl. Phys. **31**, 253 (1998).
[57]R. Peierls, Proc. Phys. Soc. **52**, 34 (1940).
[58]F. R. N. Nabarro, Proc. Phys. Soc. **59**, 256 (1947).
[59]K. Huang, *Statistical Mechanics* (Wiley, New York, 1987).
[60]K. D. Landau and E. M. Lifshitz, *Electrodynamics of the Continuous Media* (Pergamon Press, New York, 1960).
[61]R. Kaźmierkiewicz, A. Liwo, and H. A. Scheraga, J. Comput. Chem. **23**, 715 (2002).
[62]R. Kaźmierkiewicz, A. Liwo, and H. A. Scheraga, Biophys. Chem. **100**, 261 (2003); **106**, 91 (2003) (erratum).
[63]V. Muñoz and R. Ramanathan, Proc. Natl. Acad. Sci. U.S.A. **106**, 1299 (2009).
[64]See supplementary material at http://dx.doi.org/10.1063/1.4855735 for a movie of the folding trajectory of protein A at T=250 K.
[65]A. Kitao, F. Hirata, and N. Gō, Chem. Phys. **158**, 447 (1991).
[66]Y. Mu, P. H. Nguyen, and G. Stock, Proteins **58**, 45 (2005).
[67]A. Altis, P. H. Nguyen, R. Hegger, and G. Stock, J. Chem. Phys. **126**, 244111 (2007).
[68]G. G. Maisuradze, A. Liwo, and H. A. Scheraga, J. Mol. Biol. **385**, 312 (2009).
[69]U. Kozłowska, A. Liwo, and H. A. Scheraga, J. Phys. Condens. Matter **19**, 285203 (2007).
[70]R. R. Matheson and H. A. Scheraga, Macromolecules **11**, 819–829 (1978).
[71]A. Lewandowska, S. Ołdziej, A. Liwo, and H. A. Scheraga, Biophys. Chem. **151**, 1 (2010).
[72]J. F. Swain, G. Dinler, R. Sivendran, D. L. Montgomery, M. Stotz, and L. M. Gierasch, Mol. Cell **26**, 27 (2007).
[73]K. Mapa, M. Sikor, V. Kudryatsev, K. Waegermann, S. Kalinin, C. A. M. Seidel, W. Neupert, D. C. Lamb, and D. Mokranjac, Mol. Cell **38**, 89 (2010).
[74]E. I. Golas, G. G. Maisuradze, P. Senet, S. Ołdziej, C. Czaplewski, H. A. Scheraga, and A. Liwo, J. Chem. Theory Comput. **8**, 1750 (2012).
[75]U. Mayor, J. G. Grossman, N. W. Foster, S. M. V. Freund, and A. R. Fersht, J. Mol. Biol. **333**, 977 (2003).